Submicron Deformation Field Measurements: Part 3. Demonstration of Deformation Determinations

by G. Vendroux, N. Schmidt and W. G. Knauss

ABSTRACT—This is the third and last paper in a sequence devoted to an experimental investigation of deformation mechanisms at the submicron scale through the use of a specially designed scanning tunneling microscope. Its application, when used jointly with digital image correlation, as a tool for strain and deformation determinations is explored by way of two demonstrations. First, deformations in a uniaxially stressed, unplasticized (poly)vinylchloride sample are analyzed to yield the three-dimensional surface displacement field over a 10 μm × 10 μm area. Homogeneous deformations occur at the micrometer and larger size scales. However, at the 100-nm scale, inhomogeneous deformations embedded in a homogeneous deformation field appear. The second example addresses the deformation field in the vicinity of an interface between a carbon fiber and the surrounding matrix under shear stresses along the fiber. This loading leads to shearing a sheath from the carbon fiber that is about half a micron thick.

Introduction

Traditionally, two avenues present themselves to study the mechanics of very small systems. On one hand, primarily qualitative, post mortem observations are performed through high magnification microscopes, usually scanning electron or transmission electron versions. Alternately, one designs experiments which reflect macroscopically, often "on average," the effect of a theorized submicron phenomenon and then extracts the microscale phenomena by analysis under the assumption that the macroscopic measurements are uniquely related to the phenomena under investigation. Only very rarely is it possible to undertake direct quantitative micromechanical studies at the nanometer scale which could provide a definitive answer to the mechanics question at hand.

We present a demonstration of an experimental technique in micromechanics which allows surface displacements and strains to be systematically determined at the nanometer scale through a specifically designed scanning tunneling microscope (STM) and the digital image correlation (DIC) method as described previously.[1,2] (More detailed description of this work may be found in Refs. 1-6.) This paper addresses two different topics. The first arises from the desire to examine at what size scale continuum mechanical concepts might break down. Accordingly, the homogeneity of deformations at decreasing size scales is examined in a macroscopically uniaxial stress state. The material is unplasticized (poly) vinylchloride (PVC) (Specimen: Gray PVC type 1, Ain Plastics, length = 28 mm, width = 2 mm, thickness = 0.8 mm; because STMs can only image conductive surfaces, the PVC specimen was coated with a 40-nm thick layer of gold-palladium), which choice was partially motivated by the connections of this work to polymer-based adhesion studies; the other reason for this selection was the fact that the special tensile stage constructed for these studies was force limited, but had the capability to deal with a relatively low modulus material. Among these latter materials, loading of PVC could be arranged to provide near absence of relaxation-creep for the duration of the experiments (hours). Initial calibration studies with this material have been reported in Ref. 1.

Inasmuch as the details of the STM-DIC method have been documented in Refs. 1-6, it suffices to recall here that a typical scan acquired by this microscope rendered the following typical characteristics: pixel size (in-plane resolution) = 30 nm for a scan size of 300 × 300 pixels over a 9-μm × 9-μm area; the out-of-plane resolution was 8.26×10^{-3} nm. When coupled with processing data through the DIC algorithm, the error in displacement measurements resulted in deviations of ±2.5 nm for the in-plane displacements and 0.75 nm for the out-of-plane component for the same size of the scanned area.

The Scanning Tunneling Microscope and Loading Stage

One challenging aspect was to provide the STM with the capability of performing in situ straining on small but macroscopic specimens because of the perturbations that most loading systems induce, i.e., vibrations and/or specimen motion and/or temperature fluctuations. The option was displacement controlled, uniaxial tensile loading.[1,3,6] To provide the load, one grip of the load frame is physically moved while the other remains stationary. The load is measured by way of a miniature load cell (Model 31, Sensotec). Figure 1 presents the load frame with the STM.

Even with such a classically simple design, the use of the load frame-STM combination requires strict procedural constraints. Since one grip of the load frame moves, the points of the sample surface also move during loading. However, during tunneling, the STM tip is only about 1 nm away from the specimen surface so that contact between tip and surface can occur unless the changes in boundary displacements are very smooth. Because there is always some hysteresis in the piezoelectric

G. Vendroux and N. Schmidt are Graduate Students, and W. G. Knauss (SEM Member) is Professor, Graduate Aeronautical Laboratories, California Institute of Technology, Pasadena, CA 91125.

Final manuscript received: August 8, 1997.

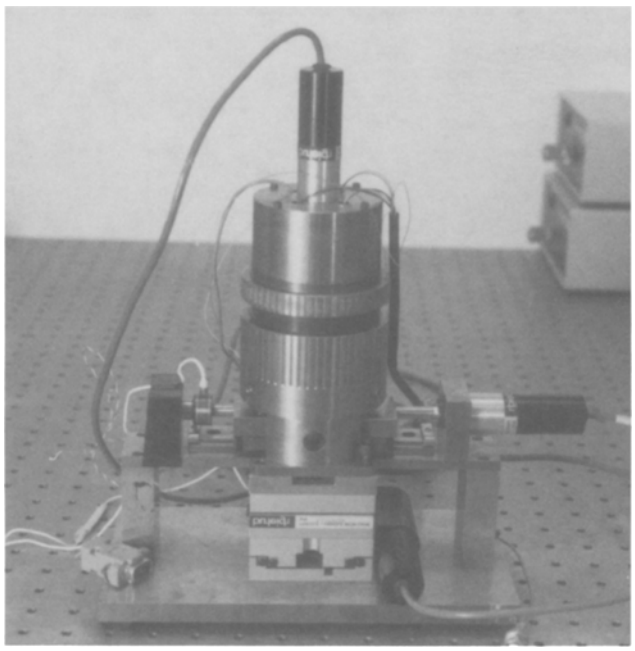

Fig. 1—The load frame under the scanning tunneling microscope. The holes in the table are spaced 1 in. apart

tube, it is difficult to retract and precisely replace the tip for each loading step on the specimen, so that the loading has to be performed with the tip in tunneling proximity. Therefore, after each loading step, the STM needs to be translated to follow the same segment of the specimen surface, which is accomplished via two high-precision translation stages of InchWorm actuators (Burleigh), with a step size of ≈ 4 nm, mounted between the specimen base and the STM. While such a device permits the loading motion to be tightly controlled (loading rate = 0.1 μm/s), it also limits the maximum load which can be transmitted to the specimen to 15 N, which in turn reflects the use of materials and/or the specimen size that can be studied with this loading stage. Moreover, the displacement field $\mathbf{U}$, computed by DIC, reflects not only the deformation of the specimen but also (possibly part of) the translation of the STM over it. The current setup does not permit the evaluation of the STM motion with the same accuracy as that of DIC so that, in this work, the data processing focuses on $\mathbf{U} - \overline{\mathbf{U}}$, where $\overline{\mathbf{U}}$ denotes the average of $\mathbf{U}$ over all points within the STM scan.

Submicron Deformation Inhomogeneities in (Poly)Vinylchloride

During initial exploration, qualitative results were pursued, so that numerical data reduction was less important. Typical loading experiments (incremental load increases) were used to examine strain and deformation behavior of PVC specimens and, in spite of small but measurable viscoelastic effects, certain surface features were identified that are indicative of microstructural changes at various load levels as evidence of the breakdown of strain homogeneity not normally admitted in continuum formulations.

Four specimens, coated with 40 nm of gold-palladium, were loaded progressively, and scans were acquired at each load with different scan windows of 9 μm × 9 μm, 6 μm × 6 μm and 3 μm × 3 μm, with the corresponding resolutions of 30 nm (the same as for the later unloading tests), 20 nm and 10 nm. In some of these tests, the scanned areas yielded small domains for which the convergence of the DIC scheme was uncharacteristically poor. Subsequently refined observations of these STM scan areas revealed the appearance of significant topographic changes under (small) load increases. Moreover, these local convergence deficiencies and the corresponding topographic changes occurred only upon first loading and did not disappear upon unloading. (Before discussing the occurrence of inhomogeneous deformations, it is prudent to alert the reader to limitations in transmitting this type of information through the printed medium. The STM naturally represents topographic height information in gray levels so that different elevations of the surface appear as either lighter or darker areas in a scan field. These features may not appear as clearly in a print as they would on a record in "false color" rendition, so that the optical impact of the data reported below may not be optimally clear in the journal reproduction.)

Figure 2 represents examples of these observed topographic differences. Features identifiable as additional dark (depression) or white ("hills") patches in the scan were acquired at the highest load (7.08 MPa) with a typical in-plane dimension on the order of 100-200 nm. However, the height of the defects, whether a dip or a crest, is 10 to 40 nm. The appearance of these topographic changes is not related to the preexisting surface profile because their occurrences arise equally in flat or in rough areas of the STM scans. Even at a stress level of only 1.5 MPa corresponding to a straining of 0.15 percent (the Young's modulus of PVC is ≈ 1 Gpa), such new topographic features were clearly detected. At such a small scale of 100-200 nm, an inhomogeneity does not represent the material bulk behavior; rather, a few polymer chains must be involved. (The radius of gyration for an isolated polymer chain is on the order of 5-10 nm.) In that sense, the size of these features may reflect the lower limit below which a standard, homogeneous (continuum) formulation for the constitutive behavior of PVC is no longer advisable.

These new topographic features are not the result of local delaminations of the gold-palladium film or strain-induced unmasking of preexisting defects. The coating on each sample surface is deposited by means of a sputter coater which produces a plasma of gold and palladium atoms in a rarefied argon atmosphere (90 mTorr). The high voltage (1.1 KV) responsible for the dissociation of the gold-palladium from the target also directs the atoms toward the specimen surface so that the gold-palladium layer is built up "atom by atom," and their local orientation and stacking creates the film structure with a loose grain size of 5-10 nm. (The reason for using

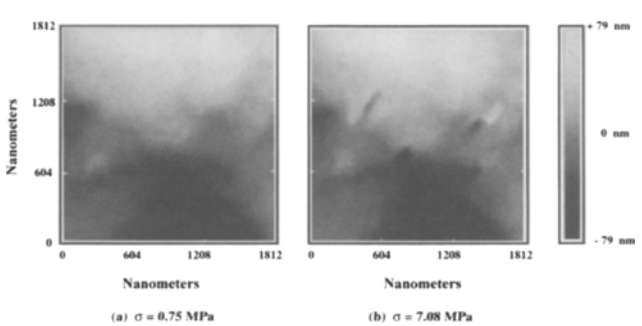

Fig. 2—Example of load-induced topographic changes on a virgin (poly)vinylchloride specimen surface

a gold-palladium coating, rather than pure gold layer, lies in the fact that the gold-palladium grain size is very much smaller than that for pure gold [50-100 nm].) Actually, the minimum thickness for a gold-palladium film to obey (continuum) conductivity laws is $\approx$ 30 nm so that the 40-nm layer can be conceptualized as gold and palladium atoms packed just sufficiently closely on the surface to allow free electron transport. It is thus an unreasonable proposition that the gold-palladium film masks the features originally and then collapses onto them as the strain increases. Moreover, if that were the case, the coating would fail, leaving non-conductive areas of the specimen exposed to the STM tip which would, in turn, cause a loss of the tunneling signal over the defect, a phenomenon that was never observed while scanning the defects. Delamination or local yielding of the coating can also be ruled out, since both depressions (holes) and local hills are created on the surface.

Once these topographical changes have occurred, no further damage can be observed at these sites under un- and reloading: the local reorganization of the polymer microstructure (chains) is irreversible. A consequence of this latter observation should be that there exists a macroscopic difference in the (uniaxial) strain-stress response of specimens between their first and subsequent loading.

Macroscopic Strain Measurements

Macroscopic strains were determined, therefore, by attaching a strain gage to a specimen (for a discussion on the use of a (mini) strain gage on PVC, refer to Ref. 1), similar to those prepared for the STM tensile experiments,[1,4,6] which was then strained in the microscope load frame in four separate tests. The first three consisted of loading the specimen through increments of about 10^{-4} m/m up to 8×10^{-4} m/m. At each strain level, the load cell and strain gage signals were recorded. The fourth test was similar, but was carried out to failure of the strain gage (1.5×10^{-2} m/m); no DIC evaluations were made. The corresponding data are presented in Fig. 3. One observes that the stress-strain response during the first loading is clearly different from that for the subsequent loadings. In fact, at a stress level of 4.5 MPa during the first loading, the specimen experiences about 4×10^{-4} m/m more strain (4 to 5 times the experimental error) than for any reloading; the second, third and fourth loadings yield identical responses up to 8×10^{-4} m/m.

These strain gage data are consistent with the inhomogeneous deformations observed above. In the virgin specimen, the polymer chains are in equilibrium with each other, but not necessarily everywhere in a minimum energy state. As the material is strained for the first time, the chains rearrange to create isolated (topographic) changes in the specimen (surface). Therefore, the strain recorded on the surface of the specimen reflects not only the elastic response of the material but also the locally permanent readjustments of (groups of) polymer chains. These rearrangements are irreversible. In reloadings to previously achieved load levels, there are fewer or no additional local molecular adjustment sites in the material, and only the (virtually) elastic response of the reordered PVC structure is reflected in the strain, and the material appears stiffer. If the stress increases beyond the maximum value experienced previously, additional rearrangements of the polymer chains take place, and the stiffness decreases further. This phenomenon is a small strain manifestation of locally nonlinear deformation characteristics which continues to occur at increased strain levels. The observed inhomogeneities may thus be considered to be the initiators of some nonlinear behavior at the microscale that becomes more pronounced at higher strain levels and to be associated with yieldlike behavior.

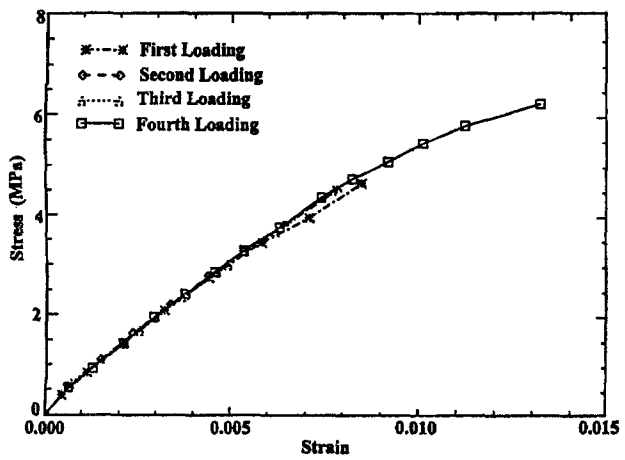

Fig. 3—Strain gage measurements on (poly)vinylchloride specimens subjected to repeated tensile loading

Displacement Field Determined by DIC

While at the 100- to 200-nm scale the deformation of the specimen can be inhomogeneous, parallel examinations showed that at and above the micron scale, continuum concepts appeared applicable. Thus, the DIC-computed deformation fields, averaged over the scan area, should reflect the macroscopic behavior.

It became clear during the above measurements that small but noticeable viscoelastic effects remained in the deformation process. This behavior was addressed in the following way. Unplasticized PVC relaxes at the rate of about 2-3 percent per decade; its time dependent Poisson behavior is not known. Although the prescription of displacement boundary conditions eliminates or minimizes in-plane creep strains, the out-of-plane deformations could lead to an artificially tilted surface scan, possibly compromising the measurements. To significantly reduce this effect, one draws on well-understood viscoelastic behavior and employs unloading histories for following the stress-strain behavior. The load is initially ramped to its maximum value (13 N) and allowed to relax for 1 h, after which time the relaxation rate has decreased to manageable levels so that at test start the load is stable. Upon unloading (typically by 4 N), the material will pursue its creep from the initial loading but also react to the new decrease in the tension; from approximatively 30 s after the load change, the two responses practically cancel each other, resulting in a stable load for about 50-70 min. This process can be repeated successfully for subsequent loading steps so that no significant artificial tilt of the image is induced. For additional issues related to data recording and processing, the reader may consult Refs. 3 and 6.

Nine in situ tensile tests (under unloading steps) were performed. In each test, three scans of the sample surface were acquired at three or four different load levels. Every image recorded was compared to the remaining two of the same specimen area at the same load through DIC in order to check

for possible scan distortions. While some of the scans suffered from image distortion attributed to hysteresis of the piezoelectric ceramic, these could be readily identified and pose a minimal problem for strain evaluations (see Ref. 3). Finally, the three topographs acquired at the highest (initial) load were correlated by DIC (scan area: 300 × 300 pixels or 9135 nm × 9135 nm with a 41 × 41 pixel subset) to all the scans recorded at subsequent (lower) loads, yielding the displacement response of the PVC specimens to load decrements. The results are presented in Fig. 4. (Because these measurements involve unloading, all the strain data are determined relative to the highest strain, the absolute value of which is not known. To compare the STM data to the strain gage readings, the microscope results were translated along the strain axis so as to match a single STM strain measurement for each experiment to the gage data.)

The agreement between the macroscopic (strain gage) and average microscopic strain is very satisfactory, especially at low strain levels (< 0.01 m/m). For higher strains (loads), the STM results tend to underestimate the strain gage readings. This trend is consistent with, if not totally explained by, the molecular model concerning the submicroscopic deformation mechanisms in PVC discussed previously. The strain-gaged specimen had been prestretched to only 0.008 m/m (4.5 MPa) prior to recording the strain readings to which the STM results are compared. Thus, for loads exceeding 4.5 MPa, new polymer structural readjustment is taking place, yielding an apparently more compliant behavior than upon unloading when such rearrangement no longer occurs.

A Study of Deformations in a Fiber Composite

As the second example for demonstrating the applicability of STM to micromechanics experiments, a study of the deformation of a carbon fiber under stress in a composite is reported. Consider a cantilever beam of unidirectional fiber-reinforced material (AS413501-6/Epoxy—Hercules prepreg—65-percent fiber, 2-percent void volume; we are grateful to Dr. James Starnes and Mr. Allan Waters of NASA-Langley for supplying these high-quality specimens) with dimensions 6 mm × 4 mm × 40 mm, clamped at one end as shown in Fig. 5 and loaded through a prescribed (end)

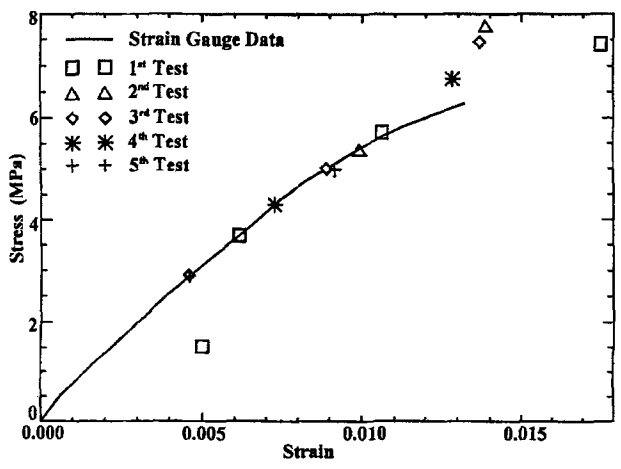

Fig. 4—Comparison of strains determined via a strain gage and the scanning tunneling microscope by Digital Image Correlation

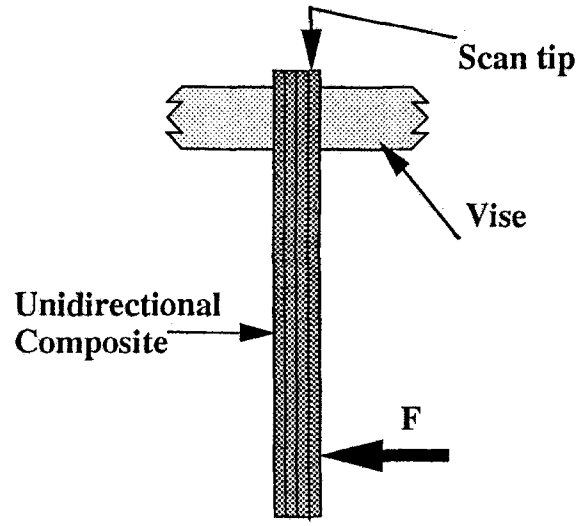

Fig. 5—Arrangement of a unidirectional composite beam in relation to the scanning tunneling microscope scan tip and the load point

displacement. As the load is increased, the fiber ends at the (clamped) beam end move relative to the matrix. While mostly tensile stresses act on the fibers in midbeam, they experience primarily shear tractions over their cylindrical surfaces at the beam end; in principle, the motion of the fiber ends relative to the matrix can thus provide information about the phase properties as a function of the distance from the matrix-fiber interface.

Specimen Preparation and Experimental Setup

To interrogate the end surface, it must be polished to maximal smoothness. Because of the markedly different hardness of the matrix and the fibers, the surface cannot be expected to be flat; considerable trial-and-error experimentation was involved in arriving at an acceptable surface condition; to make the surface sufficiently conductive for STM examination requires again the deposition of a 40-nm thick gold-palladium coating.

Polishing

Details on polishing the beam endface may be gleaned from Ref. 7, and only the net result is stated here. Best results were achieved, after initial preparation with 15- to 60-μm emery paper, with a water-based polishing compound, starting with 6-μm particles and ending up with 0.3-μm particles. These conditions still produced a relief with the fiber centers elevated by up to 150 nm above the epoxy base matrix. While a smaller relief difference would have been welcome, this condition was acceptable for the range of the STM. In addition, it provided a definitive demarcation of the matrix-fiber interface region.

Loading Arrangement

To bend the specimen while holding the end surface fixed for STM observation required a special fixture which is illustrated schematically in Fig. 6. The noteworthy features are that the specimen must be electrically isolated so that both the clamps and the load application points were made of a

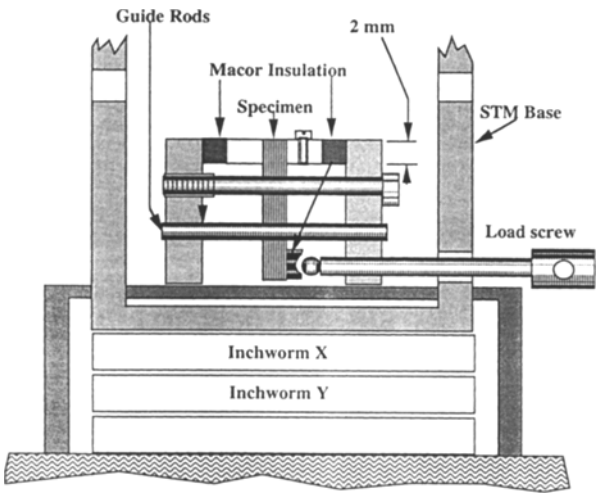

Fig. 6—Schematic of the loading fixture

ceramic (Macor) backed up by tool steel in the clamps. The displacement loading was effected through a 1/4-80 screw (0.318 mm advance per turn); one loading step consisted typically of a half turn, thus corresponding to a displacement of the cantilever beam of 0.159 mm per load increment.

Tilting of the Observation Surface

As Fig. 5 indicates, the application of a cantilever force causes the end surface of the beam to tilt. Because of the high resolution of the STM (the surface normal range is about 550 nm), the amount of tilt must be limited (< 2.5 in 100) in order to permit acquisition of profile images. At any rate, it is expected that each image contains a small amount of tilting. As for the previous measurements on PVC, the tip is kept within tunneling distance while the specimen is loaded.

Results

Next, excerpts of scans and their interpretations are presented; these are typical in the sense that the major observations recorded here apply to all the measurements made. While it is relatively easy to report the relief of the scanned surface with the aid of (artificial) color rendition, the gray-level presentation dictated by the publication process requires more explanation and study of the records. For more detail, the reader may wish to consult Ref. 7, including questions relative to identifying the location of the interface.

Figure 7 shows a selection of scan reliefs from a sequence of 15 loading steps. The upper-left-hand corner of each view represents a segment (approximately one-quarter) of the fiber cross section. Because only gray levels can be represented, some contour lines have been added in order to distinguish certain features more readily.

It is clear from Fig. 7 that the fiber occupies initially a more elevated position than the matrix. As the load increases, however, the central portion of the fiber begins to recede relative to the matrix surface, eventually withdrawing below the average of that of the matrix. However, during this process and starting at a certain load level, a portion of the fiber at the interface begins to move relative to the fiber body, thus protruding above the fiber end surface. These regions are clearly identified as the crescent-shaped features within the fiber domains. The top of the crescent in trace (d) of Fig. 7 is about 300 nm above the level of the fiber center. While the crescent shapes appear in these scans in line with the axis of compression due to the clamping of the specimen, these regions have also been observed clearly as virtually surrounding the fibers, as shown in Fig. 8 from another load sequence, so that the physical process responsible for them may not be (totally) due to the special (clamping related) stress state in the specimen (see also the discussion below relative to the studies by Drzall *et al.*[8])

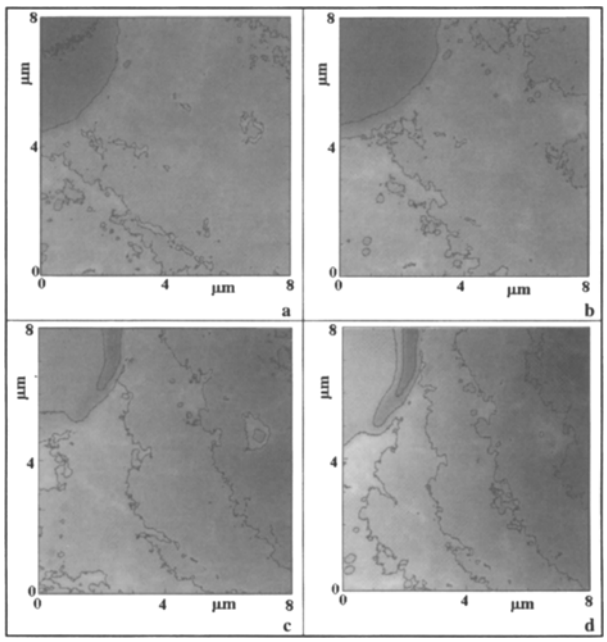

Fig. 7—A selection of scan reliefs from a sequence of 15 images. Loading: (a) nearly unloaded = step 2, (b) loading step 5, (c) loading step 11, (d) loading step 15

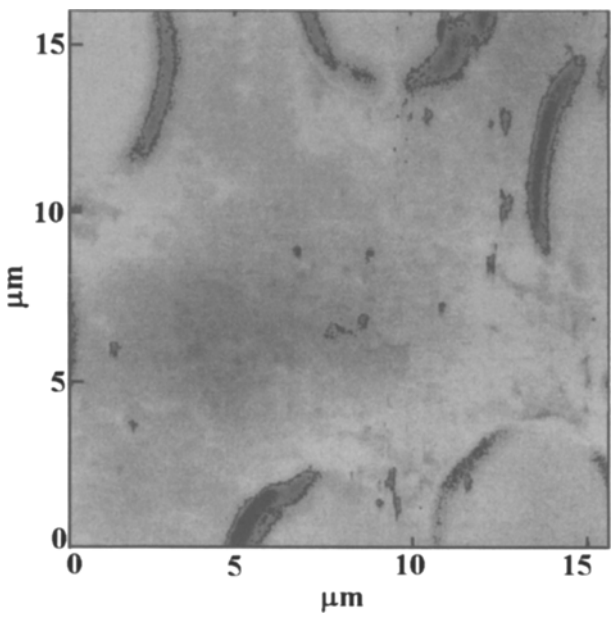

Fig. 8—An example of nearly all-around crescents from a different scan sequence than that shown in Fig. 7

These features and their load dependent evolution are recognized even more clearly in line scans which trace the height-profile along lines parallel to the two scan axes. Such profiles are shown in Figs. 9(a) and 9(b). (The left and right ends of the traces display apparently unreasonable discontinuities. These are due to the numerical scheme in the data analysis program and are of no consequence or interest here.) Following the loading steps as indicated next to the various traces, one clearly notes that (a) the center of the fiber retracts gradually with respect to the matrix and (b) following the seventh load increment, a surface segment of the fiber begins to protrude increasingly above the central portion of the fiber. Clearly, a sheath of the fiber surface has sheared off and remains attached to the matrix. This indicates that, at least in the present situation, the intrinsic shear strength of the fiber along its axis is lower than that of the interface.

It is clear that this shear-off does not follow the complete length of the fiber, but occurs in the end-near region(s). The current measurements provide no information on the length of the slipped sheath section. However, following from the significant anisotropic character of the fiber, one concludes that the broken-off pieces are not very short slivers. This observation is, perhaps, not totally surprising or unreasonable, since the fiber is itself a highly anisotropic structure with a core and skin that are markedly different.[9]

In their studies devoted to the effect of fiber surface treatment on interface slippage/failure, Drzall and coworkers[8] found that, depending on the type of surface treatment, either "clean" interfacial separation between fiber and epoxy can occur or numerous small fragments of fiber (skin) can adhere to the epoxy. The interpretation of these studies led these authors to state that this phenomenon should occur with the high-strength fibers but not so readily with the lower (axial) strength fibers involved in the present study. We must thus also raise the question whether in general shear failures attributed previously to interfacial failure are always truly clean, or whether shear failures reported previously really involve fiber failures. In the latter event, any estimate of interfacial shear strength would not be correct. To resolve this question in the general case it is necessary, as a minimum, to ensure that one also knows the location of the failure. For example, in the case of fiber pullout, the post mortem observation allows the demonstration that the failure locus was indeed interfacial. Such is not the case, however, in all situations when interfacial slip is alleged.

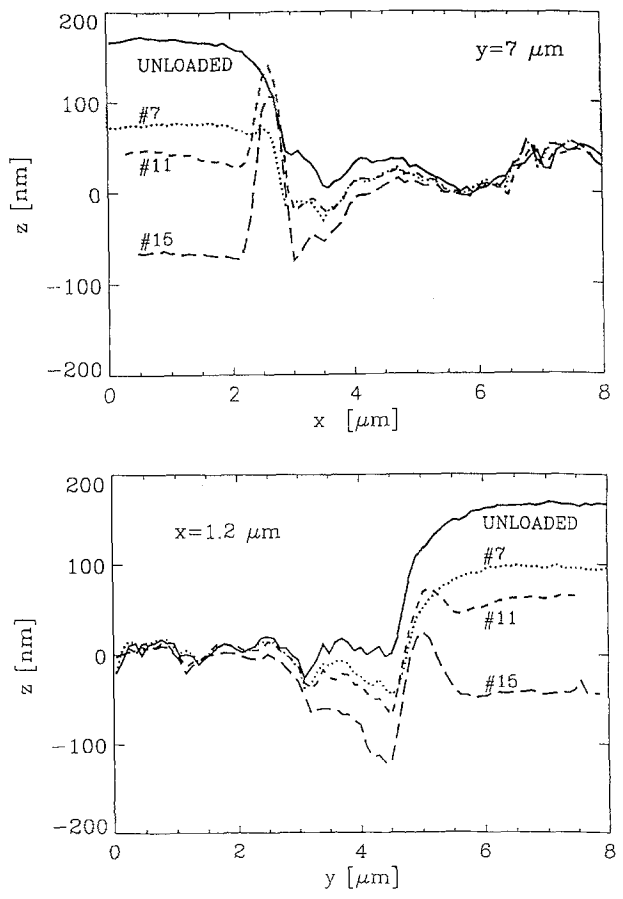

Fig. 9—Line scans from Fig. 7 illustrating the fiber sheath fracture along (a) $y = 7$ μm and (b) $x = 1.2$ μm; fiber shearing appears clearly at loading step 11

Fibrous shear failure was not always the only failure mechanism. This is shown in the next sequence of line traces. This loading sequence develops only a small fiber sheath failure but substantial interfacial shear sliding. We show first a short sequence of scans, with the small crescent region delineating fiber shear; clearly identified profiles across the scan views are given in Fig. 10, which shows the following features. First, between loading steps 8 and 10, there appears a small peak at 11 μm along the abscissa, indicating a fiber shear-off; second, note that from loading step 13 to 15 a discontinuity develops rapidly at the interface. This is evolution of slipping of the fiber relative to the matrix. Upon completely unloading the specimen (to track the specimen surface region under examination, unloading must also be accomplished in many steps), a substantial portion of this "slipped step" remains, its residual magnitude being possibly influenced by the clamping forces, which provide increased frictional tractions across the slipped surfaces.

Conclusion

The use of STM has been illustrated by two example studies: one addressed the submicroscopic evolution of inhomogeneous deformations. These are embedded in a field of deformations that appear homogeneous at a ten- to hundredfold larger size scale. The macroscopic deformations as determined with the STM agree with those determined with strain gages. The second example deals with the deformations and failure in the vicinity of fibers embedded in an epoxy matrix under (essentially) fiber parallel shear loading. It has been shown that fiber parallel shear can cause sheath fracture of the fiber, and as a consequence this failure mode must be considered in allocating causes for (near) interface failures in fiber composites. It is also demonstrated that the spatial resolution of these measurements is possibly sufficient to determine displacement gradients that can lend themselves to the potential evaluation of mechanical properties in the interface region. The spatial resolution demonstrated here, better than 20 nm, can be further heightened by a factor of at least three or four, if finer detail is desired.

It has thus been demonstrated that the STM tool can provide mechanics-relevant information at a very small size scale. This tool, as well as the atomic force microscope, is, therefore, of interest in a large number of other micromechanics-oriented problem areas, including the stress and failure responses of microelectronic devices.

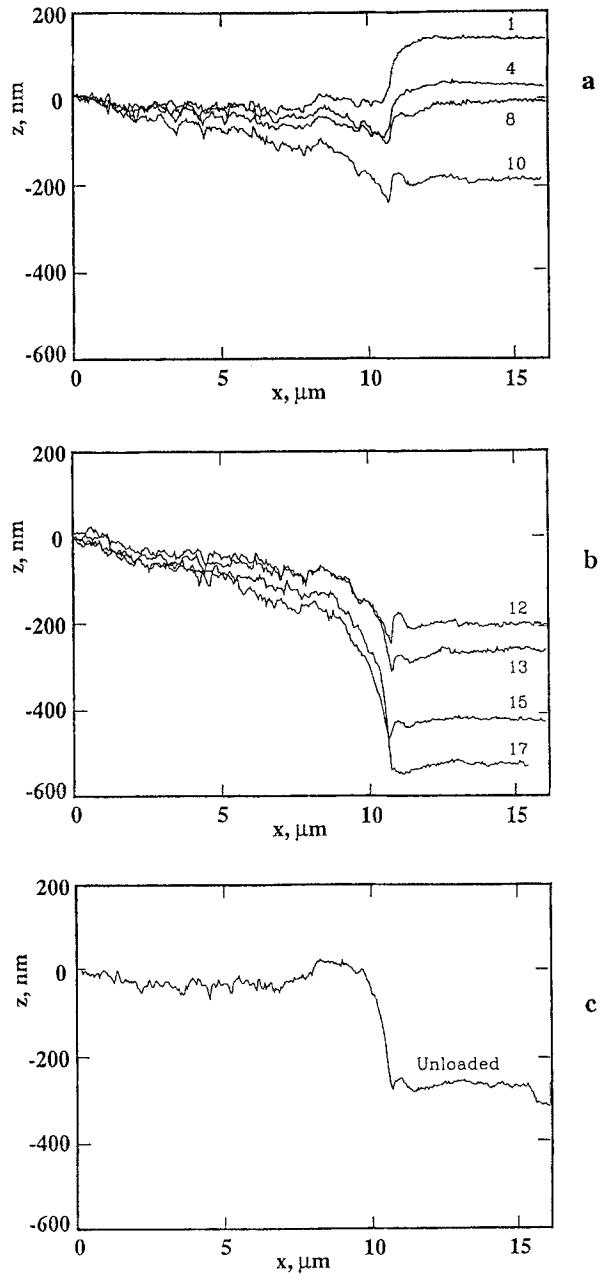

Fig. 10—A sequence of traces where fiber fracture is less pronounced (only a small crescent appears in the trace field at loading steps 12 and 13) but fiber slipping occurs around loading step 14

Acknowledgments

This work has been supported by the National Science Foundation under Grant MSS 9109973 for the hardware component of the STM. Also, substantial assistance through the Office of Naval Research (Grant N00014-91-5-1427) with Dr. Peter Schmidt as the monitor contributed to this work. The authors are indebted to Dr. M. Kinzler for his assistance in preparing the digital figures, especially for modifying the scanned fields for gray-scale printing and for finalizing the line scan traces.

References

1. Vendroux, G. and Knauss, W.G., "Submicron Deformation Field Measurements: Part 1. Developing a Digital Scanning Electron Microscope," EXPERIMENTAL MECHANICS **38**, *18–23 (1998).*

2. Vendroux, G. and Knauss, W.G., "Submicron Deformation Field Measurements: Part 2. Improved Digital Image Correlation," EXPERIMENTAL MECHANICS **38**, *86–92 (1998).*

3. Vendroux, G., "Scanning Tunneling Microscopy in Micromechanics Investigations," Doctoral thesis, GALCIT Report SM93-36, California Institute of Technology, Pasadena (1994).

4. Vendroux, G. and Knauss, W.G., "Deformation Measurements at the Sub-micron Size Scale I: Design of a Digital Scanning Tunneling Microscope," GALCIT Report SM94-4, California Institute of Technology, Pasadena (1994).

5. Vendroux, G. and Knauss, W.G., "Deformation Measurements at the Sub-micron Size Scale II: Refinements in the Algorithm for Digital Image Correlation," GALCIT Report SM94-5, California Institute of Technology, Pasadena (1994).

6. Vendroux, G. and Knauss, W.G., "Deformation Measurements at the Sub-micron Size Scale III: Deformation Mechanisms in a Structural Polymer," GALCIT Report SM94-6, California Institute of Technology, Pasadena (1994).

7. Schmid, N. "The Use of Scanning Tunneling Microscopy for a Micromechanic Investigation of the Interphase in Fiber Composites," GALCIT Report SM95-8, California Institute of Technology, Pasadena (1995).

8. Drzall, L.T., Rich, M.J., and Lloyd, P.F., "Adhesion of Graphite Fibers to Epoxy Matrices, Part I: The Role of Fiber Treatment," J. Adhesion, **16**, *1–30 (1982).*

9. Peebles, L.H., Carbon Fibers, Formulation, Structure, and Properties, CRC Press, Boca Raton, FL, Chap. 5 (1995).